International Journal of Progressive Sciences and Technologies (IJPSAT)
ISSN: 2509-0119.
© 2026 Scholar AI LLC.
https://ijpsat.org/
Vol. 60 No. 1 November 2026, pp. 528-555

Energy Performance Of A Solar Chimney Power Plant For The Electrical Supply Of A Distillation Still: Case Of Mahajanga, Madagascar

RAHARIJAONA Petera[1], DONA Victorien Bruno[2]

[1]PhD student, Doctoral School of Life Sciences and Modeling (EDGVM), University of Mahajanga, Madagascar
[2]Professor, Laboratory of Applied Physics and Renewable Energies (LPADER), Doctoral School of Life Sciences and Modeling (EDGVM), University of Mahajanga, Madagascar

Corresponding Author: RAHARIJAONA Petera. E-mail: rpetera05@gmail.com, bvdno2@gmail.com

(cc) BY

Abstract: This study evaluates the energy performance of a solar chimney power plant intended to supply electricity to a still for essential oil extraction. It aims to optimize its dimensions and operation under the climatic conditions of Mahajanga, Madagascar. The methodology combines meteorological data from 2010 to 2024, a seven-node thermal model, an electrical generation model, and an energy analysis of six experimental trials on Melaleuca, Eucalyptus and Cinnamomum. The energy requirements of the boiler, distillation vessel and condenser are evaluated to establish sizing constraints. Simulations focus mainly on January, the most restrictive month, and October, which is more favorable for solar production. Maintaining the geometric ratio of the Manzanares prototype, the reference configuration comprises a collector 180 m in diameter and a chimney 143.6 m high. It uses a 2 cm water layer, an initial boiler water volume of 250 L and the experimental durations. Simulated peak electrical powers reach 22.34 kW in January and 32.45 kW in October. Optimization involves reducing the water volume to 125 L, setting the heating period to 90 min, adjusting extraction durations and bringing forward water withdrawal. Comparison of layer thicknesses shows that a 1 cm water layer accelerates preheating. With water withdrawn at 9:24 true solar time (TST), the improved configuration comprises a 165 m collector and a 131.6 m chimney. It reduces collector area by 16.0%. For the critical 156.5 kg Eucalyptus trial, water temperatures at withdrawal are 50.62 °C in January and 65.92 °C in October. Electrical energies available during the 90 min heating period are 19.90 and 30.98 kWh, respectively, compared with estimated requirements of 9.29 and 7.15 kWh. During the 180 min extraction period, minimum electrical powers reach 15.05 and 20.46 kW, exceeding the selected sizing threshold. These results show that optimizing preheating, water volume and withdrawal time improves the match between electricity generation and process requirements. It reduces plant dimensions while meeting the energy criteria studied. The improved configuration thus demonstrates the numerical feasibility of autonomous electrical operation for the cycles considered. It is a promising solution for powering the experimental still built at the University of Mahajanga, subject to experimental validation.

Keywords: solar chimney power plant; energy performance; optimization; electricity generation; solar preheating; still; essential oils; Mahajanga.

1. INTRODUCTION

Global demand for essential oils is growing steadily, driven by the expansion of natural products in the cosmetics, perfumery, aromatherapy and pharmaceutical sectors [1], [2]. The market, valued at several billion dollars, continues to expand as consumers increasingly favor plant-derived ingredients [1], [3]. Among the most valued species are *Melaleuca quinquenervia* (niaouli), *Eucalyptus* (kininina) and *Cinnamomum camphora* (ravintsara), widely used in Madagascar and other tropical regions [4], [5].

International Journal of Progressive Sciences and Technologies (IJPSAT)
ISSN: 2509-0119.
© 2026 Scholar AI LLC.
https://ijpsat.org/
Vol. 60 No. 1 November 2026, pp. 528-555

Steam distillation remains the most widely used extraction technique, particularly at artisanal and semi-industrial scales. Although well established, this process requires substantial energy consumption: steam production generally relies on the combustion of wood or fossil fuels, resulting in high energy use and significant greenhouse gas emissions [6], [7], [8]. This energy dependence is a major obstacle to developing sustainable supply chains, particularly in rural areas where access to clean energy sources is limited. In artisanal and semi-industrial installations, this energy is most often provided by combustion.

The present work explores an alternative in which vaporization heat is supplied by an electric resistance heater powered exclusively by a solar chimney power plant sized for this purpose.

Solar chimney power plants appear to be a promising technology for converting solar energy into electricity. Based on the thermal draft generated by heating air beneath a large transparent collector, they have been widely investigated since the pioneering work of Schlaich et al. [9] and the analyses of von Backström and Gannon [10], [11]. Integrating thermal storage through a water basin beneath the collector, initially proposed by Kreetz [12] and subsequently adopted in several models [13], [14], improves system thermal inertia and extends generation beyond peak sunshine hours.

In this context, the present work proposes a physically decoupled hybrid system combining a solar chimney power plant with a full-area water basin (electrical function) and an external boiler fitted with an electric resistance heater (essential oil extraction function), based on the experimental prototype at the University of Mahajanga. The heater is the critical electrical load: it must provide both the temperature rise and maintenance of the vaporization plateau. The main objective of this work is to evaluate the energy performance of a solar chimney power plant under the climatic conditions of Mahajanga, then optimize its sizing and operating conditions to meet the still's autonomous electrical requirements during the cycles considered while making use of solar water preheating for the aromatic plants studied experimentally.

The methodology is based on the use of Mahajanga climatic data covering 2010–2024, a seven-node thermal model and an electricity generation model. Parametric analysis identifies the influence of the main geometric and thermal characteristics. Six distillation trials involving *Melaleuca, Eucalyptus and Cinnamomum* are then used to evaluate the energy requirements of the boiler and distillation vessel, together with the thermal constraints associated with the condenser. On this basis, a reference configuration is sized from the experimental conditions.

An optimization phase then focuses on reducing the initial boiler water volume, comparing various water-layer thicknesses, and adjusting operating durations and times. The analysis is carried out primarily for January, selected as the critical sizing month, and October, used to assess performance under more favorable solar conditions.

The originality of this study thus lies in combining the plant's energy sizing, solar water preheating and temporal optimization of the distillation process. It seeks to determine the conditions under which a more compact configuration can simultaneously meet the energy constraints of heating and steam production. The results aim to establish the numerical feasibility of autonomous electrical operation during the cycles studied.

2. MATERIALS AND METHODS

2.1. Presentation of the experimental prototype and characterization of input data

The study is based on the artisanal essential oil extraction unit built at the Faculty of Sciences, Technologies and Environment of the University of Mahajanga, Ambondrona Campus. The prototype is installed in a 4 m × 6 m shed enclosed with mesh on all four sides. During experimentation, heating was provided manually by burning dry wood, and the water used came from the supply network.

The boiler is a cylindrical vessel with a diameter of 0.80 m and a height of 1.00 m. A reference water mass of 250 kg is used for the energy calculations. The cylindrical distillation vessel has a diameter of 1.28 m, a height of 1.65 m and a nominal biomass capacity of 500 kg. The condenser consists of a vertical galvanized tank 0.58 m in diameter and 0.88 m high. Inspection of the

International Journal of Progressive Sciences and Technologies (IJPSAT)
ISSN: 2509-0119.
© 2026 Scholar AI LLC.
https://ijpsat.org/
Vol. 60 No. 1 November 2026, pp. 528-555

actual equipment reveals five internal tubes approximately 0.40 m long and 0.02 m in diameter. The transfer line connecting the preheated-water basin to the boiler has a measured length of 1.05 m and an outside diameter of 0.06 m.

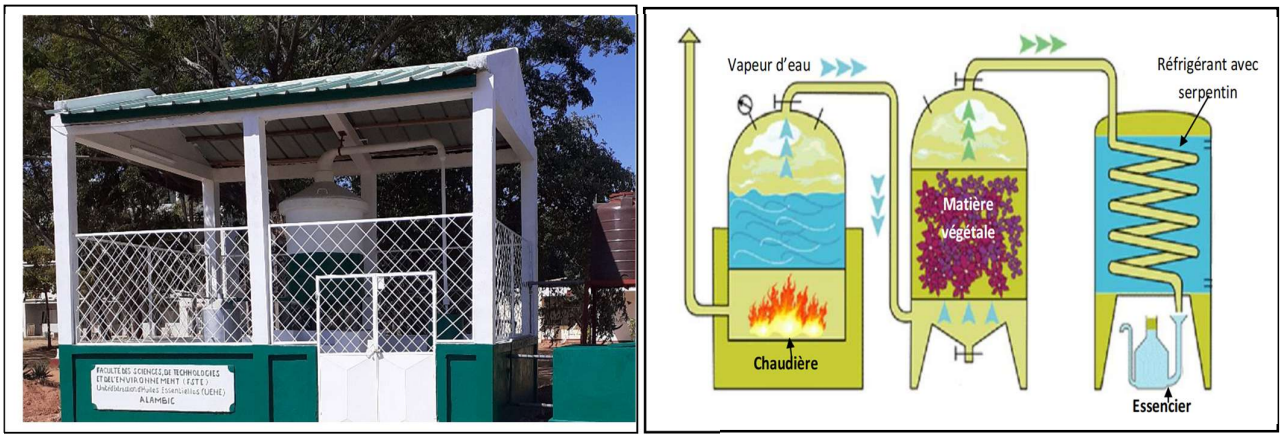


Figure 1: Experimental distillation prototype at the University of Mahajanga: photograph of the installation and schematic diagram.

Six distillation trials form the experimental basis for defining the process time constraints and production quantities. The directly measured quantities are biomass mass, heating and extraction times, essential oil volume, extraction yield, floral water volume, and the date and location of each trial. We carried out three *Eucalyptus* distillations at different times, two *Melaleuca quinquinervia d*istillations and only one *Cinnamomum camphora* distillation because this plant is rarely found in our area.

Table 1: Some plants collected for extraction

Plant names	Collection site	Distillation date	Quantity of material
Melaleuca quinquinervia (Niaouli)	Belobaka, Mahajanga II	07/06/2021	68 kg
	Belobaka, Mahajanga II	19/11/2021	96 kg
Eucalyptus sp (Kininina)	Ambondrona, Mahajanga I	18/12/2021	156, 5 kg
	Ambondrona, Mahajanga I	04/11/2021	62 kg
	BESELY, Belobaka	31/05/2021	80 kg
Cinnamomum camphora (ravintsara)	Fandriana, Amoron'i mania	14/01/2022	16 kg

The following Table 2 presents the experimental results for three types of plants collected in different quantities, recorded during each distillation. Only leaves were used.

Table 2: Experimental results

Species/load	m_bio (kg)	t_heating	t_extraction	V_HE (mL)	R_HE (%)	V_floral (L)
Melaleuca	68	49 min	2 h 21	150	0,22	16,5
Melaleuca	96	50 min	2 h 20	150	0,17	7,7
Eucalyptus	156,5	38 min	2 h 16	650	0,42	20
Eucalyptus	62	85 min	3 h 15	405	0,65	3,5
Eucalyptus	80	60 min	2 h 20	110	0,13	20
Cinnamomum	16	62 min	1 h 54	160	1,00	7

Because suitable instrumentation was unavailable, the temperature and pressure in the boiler and distillation vessel, the exact volume of water introduced in each trial, and the steam mass flow rate were not measured directly. Quantities needed for modeling but not instrumented are therefore either derived from actual geometry, adopted from the literature, estimated or calculated, or obtained by simulation. This distinction is maintained throughout the study.

2.2. Functional architecture and energy coupling of the system

The system studied relies on physical decoupling between the electricity-generation function and essential oil extraction. It comprises five main subcomponents:

- *Full-area water-basin solar collector: A circular collector is covered with a transparent cover. The entire ground surface beneath the collector is occupied by a shallow water basin. This basin provides both preheating of the water intended for the boiler and thermal storage, which stabilizes the air draft.*
- *Chimney and turbine: A chimney rises at the center of the collector. Air heated beneath the collector rises by natural draft, driving a turbine coupled to an electrical generator.*
- *External boiler: It is equipped with an auxiliary electric resistance heater, which constitutes the system's critical load. This heater receives preheated water, raises it to the required vaporization temperature and maintains that temperature throughout extraction. The heater's power demand (heating + holding stage) determines the electrical autonomy thresholds and guides the sizing of the solar chimney power plant.*
- *Distillation vessel (extraction chamber): This is the extraction reactor. It receives steam produced by the boiler. The steam then passes through the biomass bed and carries the volatile compounds.*
- *Condenser and separator: The steam + essential oil mixture is condensed and then separated. The hydrolate may optionally be recycled (cohobation) using various strategies.*

2.3. Operating principle and process sequence

In principle, the system operates through several coupled phases:

↗ *Phase 1: Solar preheating and electricity generation*

Under solar radiation, the air trapped between the glazing and the water basin heats up. The temperature difference between the warm air and ambient air creates a thermal draft in the chimney. This airflow drives the turbine and generates electricity. At the same time, the basin water progressively heats up under the solar fluxes passing through its cover.

International Journal of Progressive Sciences and Technologies (IJPSAT)
ISSN: 2509-0119.
© 2026 Scholar AI LLC.
https://ijpsat.org/
Vol. 60 No. 1 November 2026, pp. 528-555

Phase 2: Transfer of preheated water

Before each extraction process, when the plant produces more electrical energy, some of this water is transferred to the boiler through the insulated circuit according to the capacity and types of plants to be extracted.

Phase 3: Boiler heating

The electric resistance heater, powered exclusively by electricity from the solar chimney power plant, raises the water from its inlet temperature to the vaporization temperature required for extraction.

Phase 4: Vaporization holding stage and extraction

Once the vaporization temperature has been reached, the resistance heater maintains it at a constant level. The steam produced passes through the biomass in the distillation vessel, carrying volatile compounds. The mixture is then condensed and separated. The hydrolate may be recycled either to the boiler, to the basin, or later at the end of the cycle to recover dissolved essential oil. The schematic diagram and complete system configuration are presented in Figure 2 below:

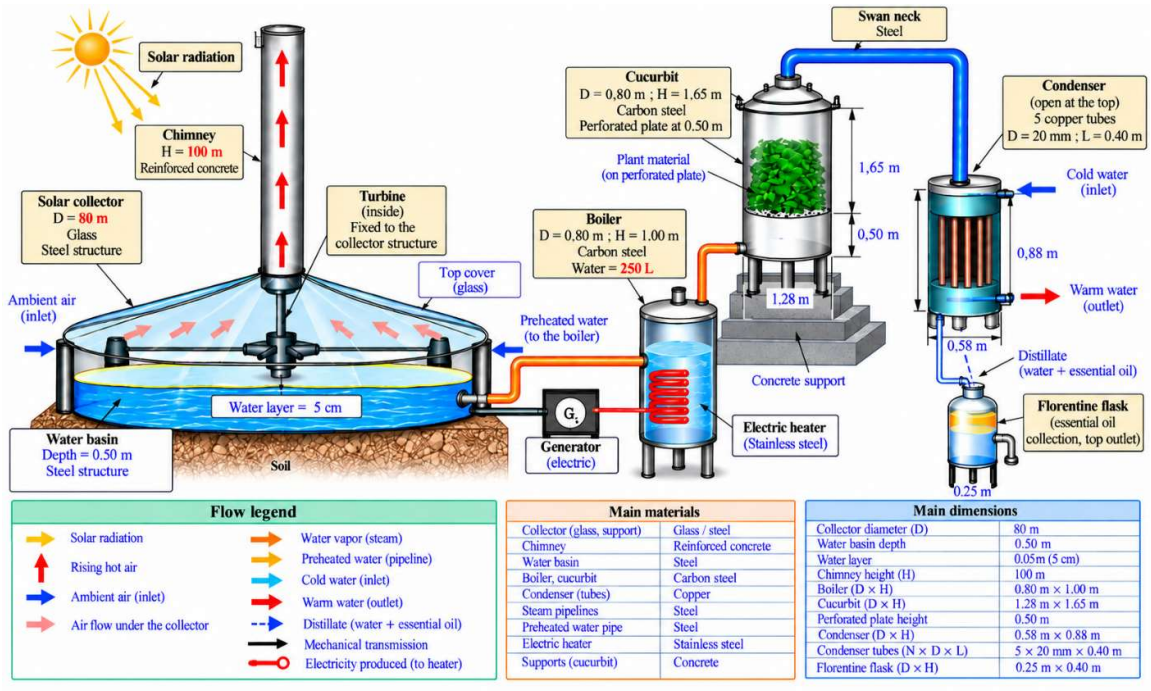


Figure 2: Schematic diagram of the proposed configuration: solar chimney power plant, external boiler and distillation unit.

2.4. Thermal-energy modeling of the subsystems

2.4.1. Thermal modeling of the solar collector with a thermal-storage water basin

Modeling heat exchange within the solar collector with a full-area water basin is based on an adaptation of the nodal model proposed by Semai [14]. To simplify the solution of the energy conservation equations, the following assumptions are adopted:

- Hybrid thermal regime: Energy balances for the upper glass, main air, intermediate plastic film, absorber, lower air and ground surface are treated as quasi-steady. By contrast, the basin water energy balance accounts for its thermal inertia through a sensible-energy accumulation term.

International Journal of Progressive Sciences and Technologies (IJPSAT)
ISSN: 2509-0119.
© 2026 Scholar AI LLC.
https://ijpsat.org/
Vol. 60 No. 1 November 2026, pp. 528-555

- Radiative exchange: The sky is treated as a blackbody characterized by an effective radiative temperature. The transparent cover is assumed opaque to thermal infrared radiation.
- Thermophysical properties: Material and fluid properties are assumed constant over the temperature ranges studied and evaluated at appropriate reference temperatures.
- Airflow: Flow in the collector is locally treated as flow between two flat plates. It is assumed axisymmetric, and azimuthal variations are neglected.
- Conductive heat transfer: Conductive transfers in the main direction of airflow are neglected relative to the convective and radiative mechanisms considered.
- Water behavior: The basin water is assumed uniform in temperature under the lumped-capacitance approach. Its energy storage is treated as sensible, without phase change.
- Evaporation: Mass and energy losses due to basin-water evaporation are neglected. The water surface is covered by a plastic film assumed to be sealed, preventing direct contact with this flow.

The collector is modeled by the seven-unknown nodal system established by Semai [14]. Convective heat transfer coefficients are calculated using the Petukhov and MacAdams correlations [15], [16], and radiative exchange is linearized using classical relationships [15].

The temperature distribution obtained from the energy balances performed on the collector is given by:

✓ Energy balance at the glazing:

$$G_1 + h_{r,vit2_vit1}\left(T_{vit2} - T_{vit1}\right) + h_{cv,vit1_air1}\left(T_{air1} - T_{vit1}\right) = h_{cv,vit1_amb}\left(T_{vit1} - T_{amb}\right) + h_{r,vit1_ciel}\left(T_{vit1} - T_{ciel}\right) \quad (1)$$

✓ Energy balance for flowing fluid 1 (air):

$$h_{cv,vit_air1}\left(T_{vitre} - T_{air1}\right) = h_{cv,abs_air1}\left(T_{air1} - T_{vit2}\right) + q''_{air} \quad (2)$$

✓ Energy balance at the plastic film:

$$G_2 = h_{cv,eau_vit2}\left(T_{eau} - T_{vit2}\right) + h_{cv,air1_vit2}\left(T_{air1} - T_{vit2}\right) + h_{r,vit1_vit2}\left(T_{vit1} - T_{vit2}\right) + h_{r,vit2_abs}\left(T_{vit2} - T_{abs}\right) \quad (3)$$

✓ Energy balance for the storage water [17], [18]:

$$h_{cv,vit2_eau}\left(T_{vit2}^{k+1} - T_{eau}^{k+1}\right) + h_{cv,eau_abs}\left(T_{abs}^{k+1} - T_{eau}^{k+1}\right) = \rho_e e_e c_{p,e} \frac{T_{eau}^{k+1} - T_{eau}^{k}}{\Delta t} \quad (4)$$

✓ Energy balance at the absorber:

$$G_3 = h_{cv,abs_eau}\left(T_{abs} - T_{eau}\right) + h_{cv,abs_air2}\left(T_{abs} - T_{air2}\right) + h_{r,abs_vit2}\left(T_{abs} - T_{vit2}\right) + U_w\left(T_{abs} - T_{abs,ref}\right) \quad (5)$$

✓ Energy balance at the thermal resistance layer:

$$h_{cv,abs_air2}\left(T_{abs} - T_{air2}\right) = h_{cv,air2_surfsol}\left(T_{air2} - T_{surf_sol}\right) \quad (6)$$

✓ Energy balance at the soil–thermal resistance layer interface:

$$h_{r,air_surfsol}\left(T_{air2} - T_{surf_sol}\right) = U_{sol}\left(T_{surf_sol} - T_{sol}\right) \quad (7)$$

The net heat flux transmitted to the flowing air can be defined in terms of the mean fluid temperature and inlet temperature, as follows [14]:

International Journal of Progressive Sciences and Technologies (IJPSAT)
ISSN: 2509-0119.
© 2026 Scholar AI LLC.
https://ijpsat.org/
Vol. 60 No. 1 November 2026, pp. 528-555

$$q''_{air} = \frac{\dot{m}_{air} C_{p,air}}{\pi r L}(T_{air} - T_{air,ent}); T_{air} = \frac{T_{air,ent} - T_{air,sort}}{2} \quad (8)$$

The heat transfer coefficient in the soil is given by the following relation [14]:

$$U_{sol} = 2\sqrt{\frac{k_{sol}\rho_{sol}C_{p,sol}}{\pi t}} \quad (9)$$

Heat exchange within the water layer is estimated using a natural-convection correlation based on the Rayleigh and Nusselt numbers. The formulation adopted corresponds to the horizontal form of the correlation proposed by Hollands et al. [19]:

The Rayleigh number is $Ra_e = \frac{g\beta_e \Delta T_e e_e^3}{\nu_e \alpha_e}$ où $\Delta T_e = \max(T_{abs} - T_{pf,0})$ (10)

The Nusselt number used is: $Nu_e = 1 + 1,44\left(1 - \frac{1708}{Ra_e}\right) + \left[\left(\frac{Ra_e}{5830}\right)^{1/3} - 1\right]_+$ (11)

The Rayleigh number is defined from the water-layer thickness, the temperature difference between its bounding surfaces, and the thermophysical properties of water. The Nusselt number then enables estimation of the layer's equivalent thermal conductance.

The instantaneous thermal power stored in the basin (dynamic regime), derived directly from the energy balance for a lumped-capacitance system, can be expressed as [15]:

$$\dot{Q}_{th,eau}(t) = m_{eau,bac}.c_{p,eau}.\frac{dT_{eau}}{dt} \quad (12)$$

When preheated water is withdrawn toward the boiler, the useful thermal power during transfer to the boiler is written as:

$$\dot{Q}_{transfert} = \dot{m}_{transfert}.c_{p,eau}.(T_{eau} - T_{ref,chaudiere}) \quad (13)$$

2.4.2. Aerodynamic and electrical modeling of the chimney and turbine

The aerodynamic and electrical modeling of the plant is based on the principles of mass and energy conservation and on a simplified representation of thermal draft in the solar chimney. The simplifying assumptions are as follows [20], [21], [22]:

- Air is treated as an ideal gas, and its density is evaluated from its temperature and atmospheric pressure.
- Flow in the chimney is assumed one-dimensional and quasi-steady at each time step.
- Density variations are taken into account when evaluating the thermal draft under the Boussinesq approximation.
- The air temperature at the chimney inlet is equated to the main air temperature obtained at the collector outlet.
- Distributed and local pressure losses are neglected in the ideal aerodynamic model.
- The driving pressure is divided between the kinetic energy of the flow and the pressure extracted by the turbine.
- The ratio of pressure extracted by the turbine is set to two thirds of the available driving pressure.
- The combined turbine and generator efficiency is assumed constant and equal to 80%.

- The air mass flow rate is determined iteratively, taking account of temperatures from the thermal model.

❖ ***Collector thermal efficiency:***

The collector thermal efficiency can be expressed as the ratio of the heat power gained by the air to the solar energy supplied to the collector [23]:

$$\eta_{coll} = \frac{Q_{coll}}{G_{coll}}, \quad \eta_{coll} = \alpha - \frac{\beta}{G_H}\Delta T_{coll} \tag{14}$$

$$\text{Where } Q_{coll} = \dot{m} C_p \Delta T_{coll} = \alpha A_{coll} G_H - \beta A_{coll} \Delta T_{coll} \tag{15}$$

The air mass flow rate at the chimney inlet can be calculated by:

$$\dot{m} = \rho_{coll} \times A_{chem} \times V_{air,chem} \tag{16}$$

❖ ***Chimney thermal efficiency***

According to Jörg Schlaich, chimney efficiency is expressed as follows [24]:

$$\eta_{chem} = \frac{P_{tot}}{Q_{coll}} = \frac{g \times H_{chem}}{Cp \times T_{amb}} \tag{17}$$

Using the Boussinesq approximation for an ideal gas, the air velocity at the chimney inlet is [25]:

$$V_{ch} = \sqrt{\frac{2gH_{chem}}{3}\frac{\Delta T_a}{T_{amb}}}, \quad \Delta T_a = T_{air1} - T_{amb} \tag{18}$$

The total airflow power can be expressed as:

$$P_{tot} = \rho_{air} g H_{chem} \frac{\Delta T}{T_{amb}} V_{ch} S_{chem} \tag{19}$$

❖ ***Electrical power produced by the solar chimney power plant [26]***

This is the net power delivered. It can be expressed as the maximum mechanical power recovered at the turbine shaft multiplied by turbine efficiency:

$$P_{CCS,elec} = \eta_{turb} \times P_{tur,max} \tag{20}$$

Maximum mechanical power extracted by the turbine is attained when the pressure drop across the turbine equals two thirds of the total available pressure difference:

$$P_{tur,max} = \frac{2}{3}\eta_{coll}.\eta_{chem}.G.S_{coll} \tag{21}$$

Thus, the power generated by the solar chimney is proportional to the collector area and chimney height and therefore proportional to the volume of a cylinder with a base equal to the collector area and a height equal to that of the stack:

$$P_{CCS,elec_max} = \frac{2}{3}\eta_{Turb}.\eta_{coll}.\frac{g.H_{chem}}{C_{p,air}.T_{amb}}.G.S_{coll} \tag{22}$$

International Journal of Progressive Sciences and Technologies (IJPSAT)
ISSN: 2509-0119.
© 2026 Scholar AI LLC.
https://ijpsat.org/
Vol. 60 No. 1 November 2026, pp. 528-555

❖ ***Overall electrical efficiency:***

$$\eta_{global} = \frac{P_{elec}}{G.S_{coll}} \quad (23)$$

2.4.3. Thermal model of the external electric boiler

The external electric boiler is modeled using the energy conservation principle and a lumped-capacitance approach. This method draws on electric-boiler thermal models developed by Farooq et al. (2015), as well as transient thermal modeling principles presented by Bergman et al. (2018) [28], [29]:

$$C_{eq}.\frac{dT_{ch}}{dt} = P_{res}(t) - UA_{ch}.(T_{ch} - T_{amb}) \;;\; C_{eq} = m_{eau}.c_{p,eau} + m_p.c_{p,p} \quad (24)$$

For constant resistance-heater power, the analytical solution is written as:

$$T_{ch}(t) = T_{amb} + \frac{P_{res}}{UA} + \left(T_{sortie} - T_{amb} - \frac{P_{res}}{UA}\right)e^{-t/\tau} \quad (25)$$

where the time constant is defined by $\tau = C_{eq} / UA$

The heating and holding-stage powers are determined from the experimental data in Table 2. The heating-phase balance accounts for heating the water and the thermal inertia of the metal shell. The power that must be supplied by the electric resistance heater is estimated by distinguishing two successive phases [15], [27], [28], [29], [30]:

- **Heating phase (rise to T_vap):**

$$E_{chauffe} = Q_{eau,sensible} + Q_{pertes}$$

$$Q_{eau,sensible} = \dot{m}_{eau}\, C_{p,eau}(T_{vap} - T_{préchauf}) + m_p.C_{p,p}(T_{vap} - T_{amb}) \quad (26)$$

$$Q_{pertes} = \int_{t_0}^{t_1} UA\left(\frac{T_{eau,0} + T_{vap}}{2} - T_{amb}\right)dt$$

$$P_{chauffe} = E_{chauffe} / t_{chauffe} \quad (27)$$

- **Holding stage (steam production for extraction)**

During extraction, the minimum thermal power for phase change is:

$$P_{Palier} = \dot{m}_{vap}\, \Delta H_{vap} \quad (28)$$

Where the steam flow rate is estimated from the floral water volume and ≈ 2257 kJ·kg⁻¹ is the vaporization enthalpy $\dot{m}_{vap}\ \Delta H_{vap}$

2.4.4. Geometric, hydrodynamic and energy modeling of the distillation vessel

The distillation vessel constitutes the extraction reactor. It receives steam produced by the boiler.

- ***Geometric analysis***

The internal volume of the distillation vessel is calculated using the conventional cylinder relation:

$$v = \pi\left(D/2\right)^2 H_{utile} \quad (29)$$

The apparent bulk density ρapp and porosity ε are determined for each biomass load mbio according to [31]:

$$\rho_{app} = m_{bio} / v_{lit}, \qquad \varepsilon = 1 - (\rho_{app} / \rho_{réelle}) \quad (30)$$

Where the volume actually occupied by the plant bed is indicated and ρreal is the true density of the leaves. v_{lit}

The steam mass flow rate is estimated from the floral water volume collected. The superficial velocity u_0 and mean residence time τ are expressed by [31]:

$$u_0 = \frac{\dot{m}_v}{\rho_v S}, \qquad \tau = \frac{\varepsilon H_{lit}}{u_0} \quad (31)$$

with the cross-sectional area and ρv the saturated-steam density. $S = \pi(D/2)^2$

- ***Energy balance***

The thermal power associated with the steam flow rate is written as:

$$\dot{Q}_{vapeur} = \dot{m}_v .\Delta H_{vap} \quad (33)$$

- ***Sensible energy absorbed by the biomass [32]:*** $E_{bio} = m_{bio} c_{p,bio} (T_f - T_i) / 3600$ (34)
- ***Energy absorbed by the metal wall [33]:*** $E_{paroi} = m_c c_{p,c} (T_f - T_i) / 3600$ (35)
- ***Thermal losses from the distillation vessel:*** $E_{pertes} = \frac{1}{1000} \int_{t_0}^{t_f} U_c A_c (T_s - T_{amb}) dt$ (36)
- ***Specific latent vaporization energy per unit plant mass***

The specific extraction energy for the complete cycle is defined by [34]:

$$e_{sp} = E_{cycle} / m_{bio} \quad \text{avec} \quad E_{cycle} = E_{chauffe} + P_{palier} .t_{ext} \quad (37)$$

2.4.5. Thermal modeling of the condenser

The condenser studied consists of five vertical copper tubes, with an outside diameter of approximately 20 mm and a useful length of approximately 0.40 m. The total external heat transfer area is:

$$A = N.\pi.D_0.L \quad (38)$$

The thermal power to be removed is determined by the steam flow rate produced during the holding stage [15]:

$$\dot{Q}_{cond} = \dot{m}_{vapeur} .L_{vap} + \dot{m}_{vapeur} .c_{p,l} (T_{vap} - T_{cond,sortie}) \quad \text{où} \quad L_{vap} \approx 2257 \text{ kJ kg}^{-1} \quad (39)$$

The water flow required to remove the condensation heat is obtained from a sensible-energy balance on the cooling water [35], [36]:

International Journal of Progressive Sciences and Technologies (IJPSAT)
ISSN: 2509-0119.
© 2026 Scholar AI LLC.
https://ijpsat.org/
Vol. 60 No. 1 November 2026, pp. 528-555

$$\dot{Q}_{cond} = \dot{m}_{eau} . C_{p,eau} \Delta T_{eau}$$

$$\dot{m}_{eau} = \dot{Q}_{cond} / (C_{p,eau} \Delta T_{eau}) \quad (40)$$

The required heat transfer capacity is assessed from the overall heat transfer coefficient:

$$Q_{cond} = U.A.\Delta T_{lm} \quad \text{soit} \quad U = Q_{cond} / A.\Delta T_{lm} \quad (41)$$

where the overall heat transfer coefficient and the logarithmic mean temperature difference are indicated.$U\Delta T_{lm}$

The required number of cylindrical tubes is obtained by:

$$N_{tubes} = \frac{\dot{Q}_{cond}}{U \Delta T_{lm} \pi . D_0 . L} \quad (42)$$

2.5. Energy-autonomy criteria and geometric sizing procedure

The solar chimney power plant is sized by comparing simulated electricity generation with the energy requirements of the distillation process. This approach follows the sizing principles of solar systems intended for industrial processes, for which the temporal distribution of the energy resource and that of demand are decisive parameters (Franco, 2020; Schoeneberger et al., 2020). The following assumptions are adopted [37], [38], [39]:

- ✓ The plant's electrical generation varies during the day according to meteorological conditions.
- ✓ Boiler operation is divided into two successive stages: raising the temperature of preheated water and producing steam for extraction.
- ✓ During heating, sizing is based on the electrical energy available over the period considered.
- ✓ During extraction, the electrical power available must be sufficient to ensure continuous steam generation.
- ✓ No electrical storage is considered. Sensible energy accumulated in boiler water during heating is distinguished from the energy generated by the power plant.
- ✓ January is selected as the unfavorable reference climatic period among the conditions studied.
- ✓ Chimney height is determined from a constant geometric ratio between its height and the collector diameter, obtained from the dimensions of the Manzanares experimental prototype (Schlaich et al., 2005).
- ✓ The selected configuration is the smallest geometry meeting the energy criteria among those examined, under the numerical-model assumptions.

The sizing procedure directly uses the time-dependent electrical power profile calculated for the solar chimney power plant. During heating, the condition is satisfied when the cumulative electrical energy reaches the heating requirement:

$$\eta_R \int_{t_0}^{t_1} P_{el,disp}(t) dt \geq E_{chauffe,req} \quad (43)$$

Where: electrical power available to the boiler; efficiency of conversion of electricity into useful heat; thermal energy required for the heating stage; start and end times of heating $P_{el,disp}$ η_R $E_{chauffe,req}$ t_o et t_1

The extraction stage then begins, and the electrical power available must remain above the required vaporization power:

$$P_{el,disp}(t) \geq P_{el,req}(t) \quad \forall t \in \left[t_{ext,d} - t_{ext,f} \right] \quad (44)$$

Thus, $P_{el,req}(t) = \frac{E_{chauffe}}{\eta_R}$ (45)

To determine a configuration capable of reproducing the conditions observed in the six experimental trials, sizing is based on a geometric relationship from the Manzanares experimental prototype. With a collector diameter of approximately 244 m and chimney height of 194.6 m, the corresponding geometric ratio is:

$$\lambda = \frac{H_{chem}}{D_{col}} = \frac{194,6}{244} = 0,7975 \quad (46)$$

λ is a geometric ratio observed on a reference installation

For each candidate collector diameter D_col, the corresponding height is determined by:

$$H_{chem} = 0,7975.D_{col} \quad (47)$$

3. RESULTS AND DISCUSSION

3.1. Characterization of the solar resource and identification of the sizing month

Analysis of Mahajanga meteorological data for 2010–2024, obtained from the ASECNA Amborovy Mahajanga meteorological station, reveals substantial solar and temperature resources. Mean sunshine duration reaches 255.43 h per month, or approximately 8.40 h per day.

Figure 3 shows that January has the most restrictive conditions among the months studied, with 169.49 h of sunshine per month, or 5.46 h per day. Maximum solar irradiance reaches 655.57 W·m^{-2} at approximately 12.60 h TST. Ambient temperature varies from approximately 26.05 to 31.50 °C, whereas apparent sky temperature ranges from 12.53 to 20.38 °C. Mean wind speed is around 3.60 to 4.37 m·s^{-1}. Conversely, October is a favorable month, with maximum solar irradiance of 949.57 W·m^{-2} around 12.20 h TST. Ambient temperature then ranges from approximately 25.62 to 33.74 °C. This contrast between January and October justifies selecting January as the critical sizing month.

International Journal of Progressive Sciences and Technologies (IJPSAT)
ISSN: 2509-0119.
© 2026 Scholar AI LLC.
https://ijpsat.org/
Vol. 60 No. 1 November 2026, pp. 528-555

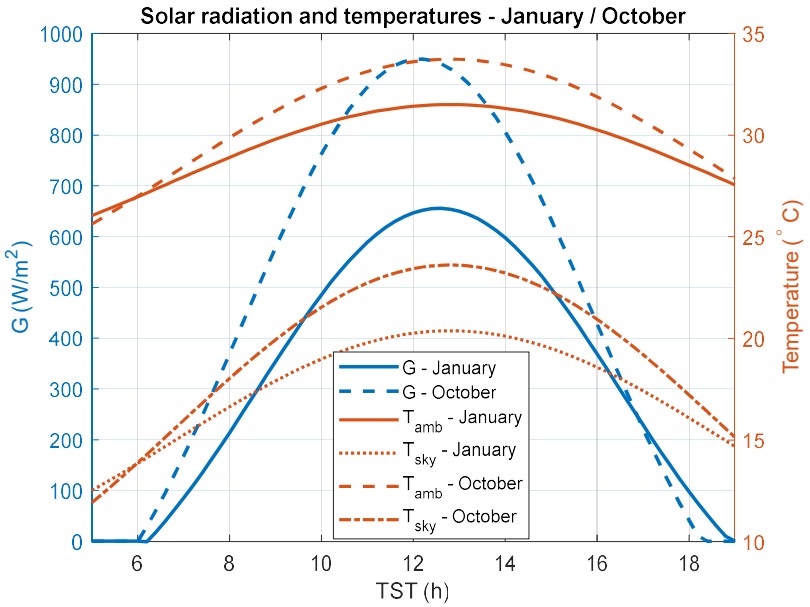


Figure 3: Representative hourly profiles of solar irradiance, ambient temperature and apparent sky temperature in January and October in Mahajanga.

3.2. Simulated thermoelectric performance of the initial configuration

The configuration used to characterize the behavior of the solar power plant comprises a collector 80 m in diameter, a chimney 100 m high and a 5 cm water layer. This configuration serves as the basis for the thermal and energy analysis before sizing for the extraction process.

3.2.1. Hourly evolution of the temperatures of the seven collector nodes

Figure 4 presents the time evolution of temperatures at the seven thermal nodes of the solar collector for typical January and October days, established from meteorological data for Mahajanga.

In January, maximum temperatures reach 37.48 °C for the upper glazing, 42.07 °C for the main air, 59.41 °C for the plastic film, 60.35 °C for the water, 61.34 °C for the absorber, 58.98 °C for the lower air and 56.62 °C for the soil, respectively. In October, temperatures are higher, with corresponding maxima of 42.45 °C, 48.04 °C, 72.98 °C, 74.21 °C, 75.54 °C, 72.14 °C and 68.74 °C. This evolution is mainly explained by the increase in incident solar irradiation. The absorber has the highest peak temperatures, consistent with its role in absorbing transmitted solar radiation. The plastic film and water display temperatures close to that of the absorber. This time lag notably reflects the thermal inertia of the water, represented by a sensible-energy accumulation term in the numerical model. The maximum water temperature rises from 60.35 °C in January to 74.21 °C in October, a difference of 13.86 °C. These results show that solar availability strongly influences the preheating potential of the water intended for the external boiler.

International Journal of Progressive Sciences and Technologies (IJPSAT)
ISSN: 2509-0119.
© 2026 Scholar AI LLC.
https://ijpsat.org/
Vol. 60 No. 1 November 2026, pp. 528-555

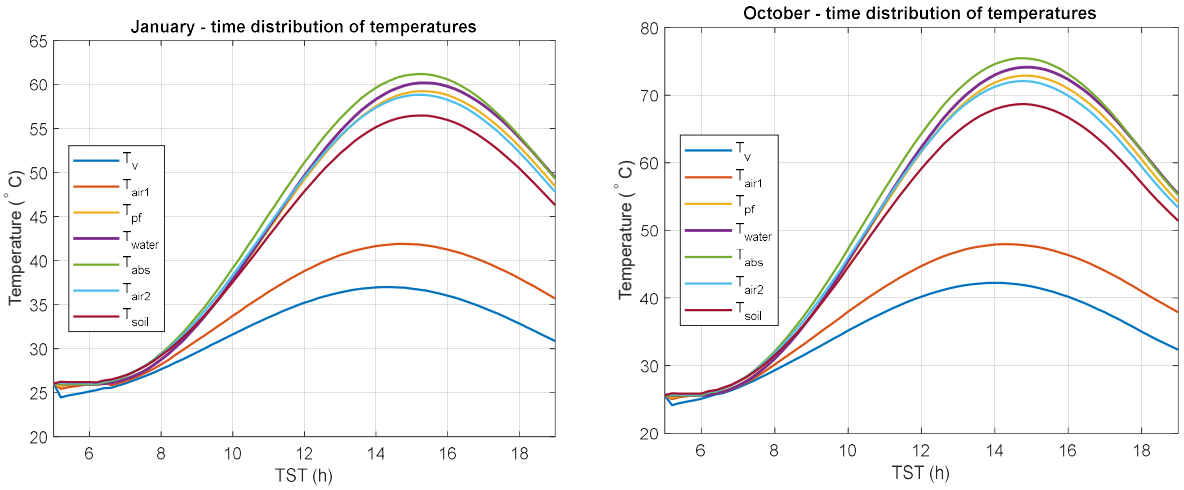


Figure 4: Hourly evolution of simulated temperatures at the seven collector nodes in January and October

3.2.2. Simulated thermal and electrical powers and plant efficiencies

Figure 5 shows that the thermal power transferred to the collector air reaches 2 MW in January and 2.89 MW in October. The corresponding maximum electrical power is 3.38 kW in January and 4.89 kW in October. According to Figure 6, maximum electrical power occurs around solar noon, whereas water temperature continues to increase for several hours. In January, peak power occurs at approximately 12.40 h, while maximum water and air temperatures are not reached until 15.40 h. This time difference confirms the temporal decoupling between electricity generation, linked to instantaneous solar flux, and thermal storage, governed by energy accumulation in the water.

Figure 7 shows that average collector thermal efficiency remains close to 60%, whereas the overall system efficiency is around 0.10%. The plant uses a small temperature difference and converts only a small fraction of the available heat into mechanical and then electrical energy.

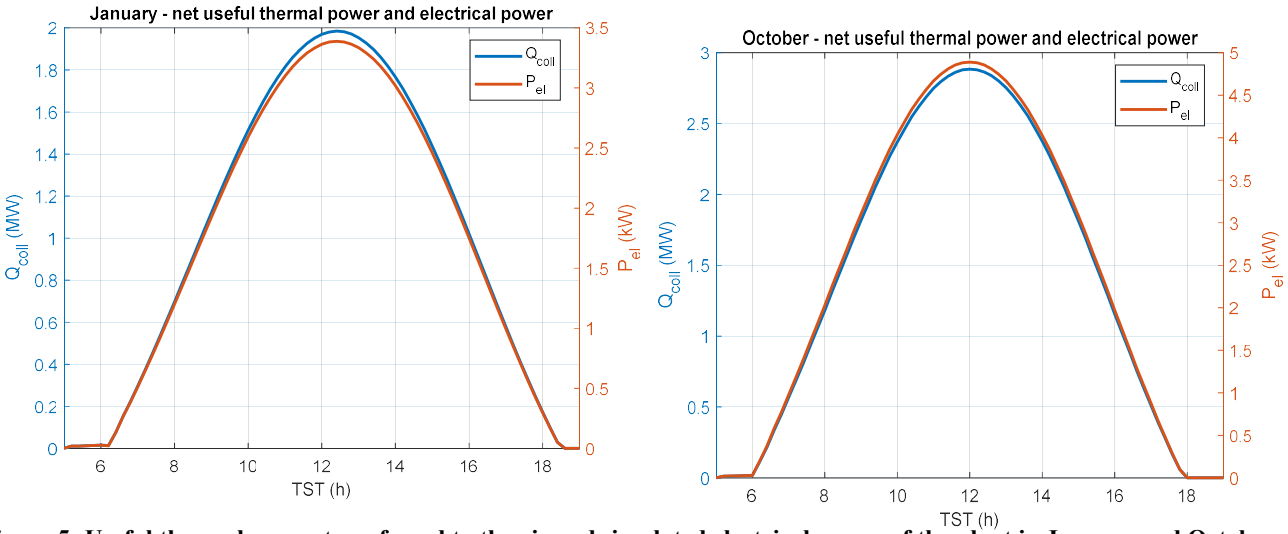


Figure 5: Useful thermal power transferred to the air and simulated electrical power of the plant in January and October.

International Journal of Progressive Sciences and Technologies (IJPSAT)
ISSN: 2509-0119.
© 2026 Scholar AI LLC.
https://ijpsat.org/
Vol. 60 No. 1 November 2026, pp. 528-555

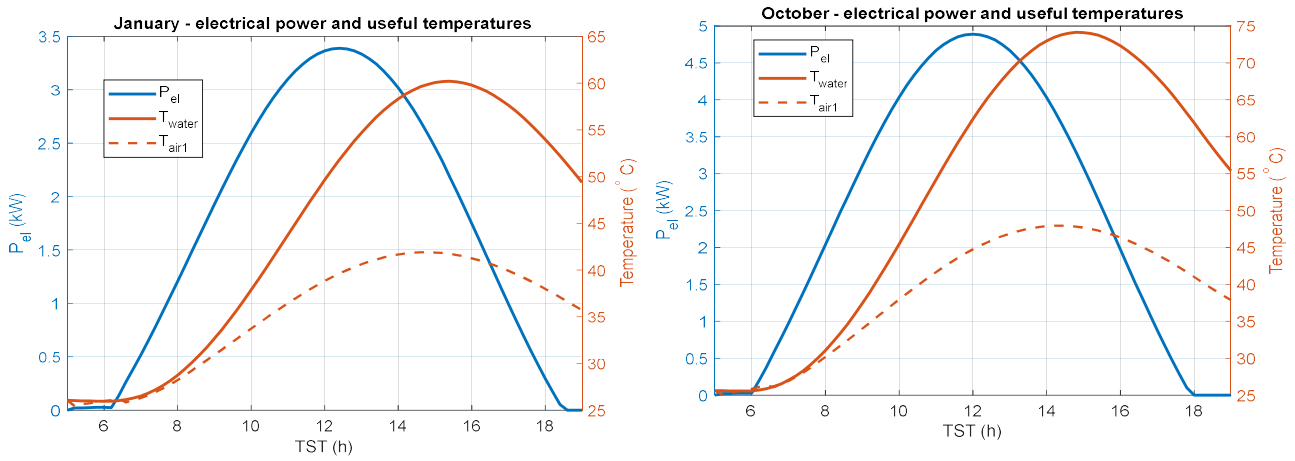


Figure 6: Hourly profiles of simulated electrical power, stored-water temperature and main air temperature in January and October.

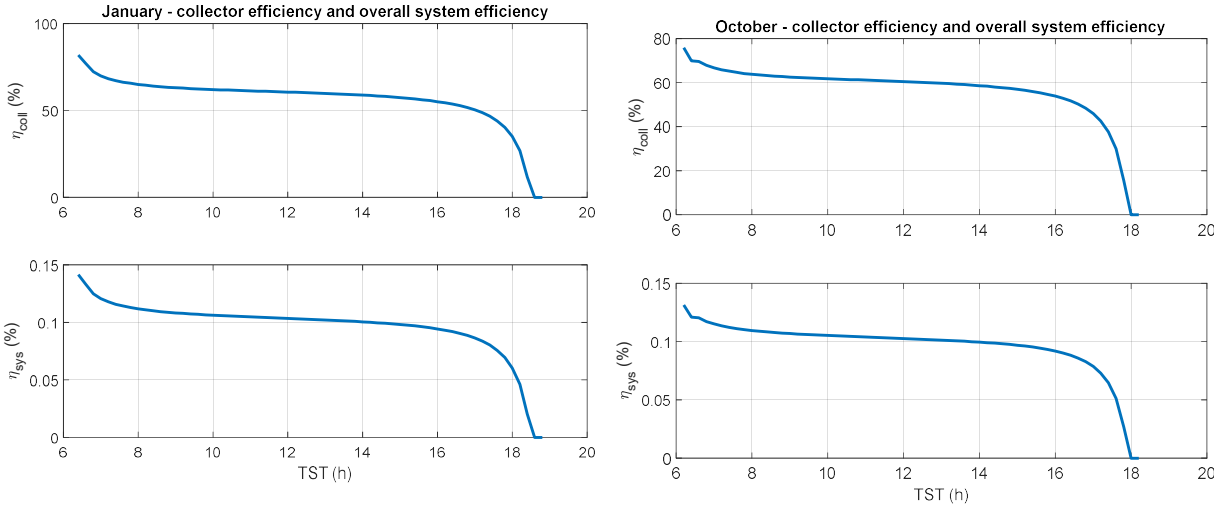


Figure 7: Hourly evolution of simulated collector thermal efficiency and overall electrical efficiency in January and October.

Figure 8 shows the net thermal storage power of the water as a function of its temperature in the basin. A positive value corresponds to energy accumulation in the water. A zero value corresponds to the maximum temperature, whereas a negative value indicates cooling or thermal discharge.

In January, the net storage power becomes zero at about 15.40 h and in October at about 15.20 h. These times correspond to the maximum water temperatures. This evolution confirms that the basin acts as sensible thermal storage. During the first part of the day, the water accumulates some of the solar energy received. After its thermal maximum, it gradually begins to release this energy.

International Journal of Progressive Sciences and Technologies (IJPSAT)
ISSN: 2509-0119.
© 2026 Scholar AI LLC.
https://ijpsat.org/
Vol. 60 No. 1 November 2026, pp. 528-555

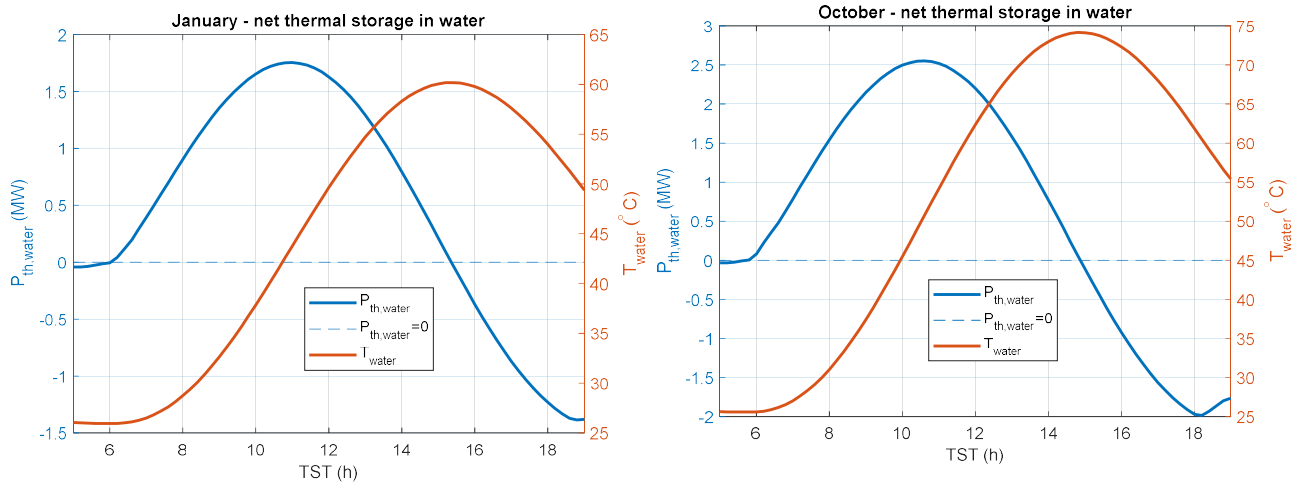


Figure 8: Hourly evolution of net thermal storage power and mean basin-water temperature in January and October

3.2.3. Sensitivity analysis of system parameters

The sensitivity study is carried out under mean October climatic conditions to identify the parameters affecting water preheating and electricity generation. Four parameters are examined: water-layer thickness, imposed water temperature, collector diameter and chimney height.

When water-layer thickness increases from 2 to 10 cm, the maximum temperature falls from 87.14 to 60.14 °C, a reduction of 27.00 °C (Fig. 9a). Meanwhile, the time of the maximum is delayed from 13.60 to 16.00 h. Greater thickness increases water mass and thermal capacity, tending to slow the temperature rise and delay the thermal peak. Conversely, thin layers favor a faster thermal response. However, maximum electrical power increases slightly from 4.74 to 5.02 kW, or approximately 5.9%. These results show that thickness mainly affects water thermal inertia, whereas its effect on electrical power remains relatively limited.

When imposed water temperature increases from 50 to 80 °C, maximum main air temperature rises from 40.67 to 50.34 °C, or 9.67 °C (Fig. 9b). Over the same range, maximum electrical power decreases slightly from 5.00 to 4.75 kW, or approximately 5.0%. This trend highlights the influence of thermal interactions between the water and main air within the adopted model.

The influence of collector diameter is much more pronounced. At a constant chimney height of 100 m, increasing the diameter from 80 to 125 m raises maximum electrical power from 4.89 to 11.72 kW, an increase of approximately 139.7% (Fig. 9c). By contrast, maximum water temperature increases moderately from 74.21 to 76.77 °C, or 2.56 °C. This evolution is mainly due to the increase in solar collection area.

At a constant collector diameter of 80 m, increasing chimney height from 50 to 150 m raises maximum electrical power from 2.43 to 7.37 kW, or approximately 203.5% (Fig. 9d). Conversely, maximum water temperature decreases slightly from 75.23 to 73.63 °C, a difference of 1.60 °C. Increasing height thus favors estimated electricity generation by increasing the potential for thermal draft, while its influence on water temperature remains limited.

Overall, the sensitivity analysis shows that water-layer thickness mainly influences the basin's thermal dynamics, whereas collector diameter and chimney height are the main geometric parameters affecting calculated electrical power. From a sizing standpoint, the most effective levers for electrical power are D_col and H_chem.

International Journal of Progressive Sciences and Technologies (IJPSAT)
ISSN: 2509-0119.
© 2026 Scholar AI LLC.
https://ijpsat.org/
Vol. 60 No. 1 November 2026, pp. 528-555

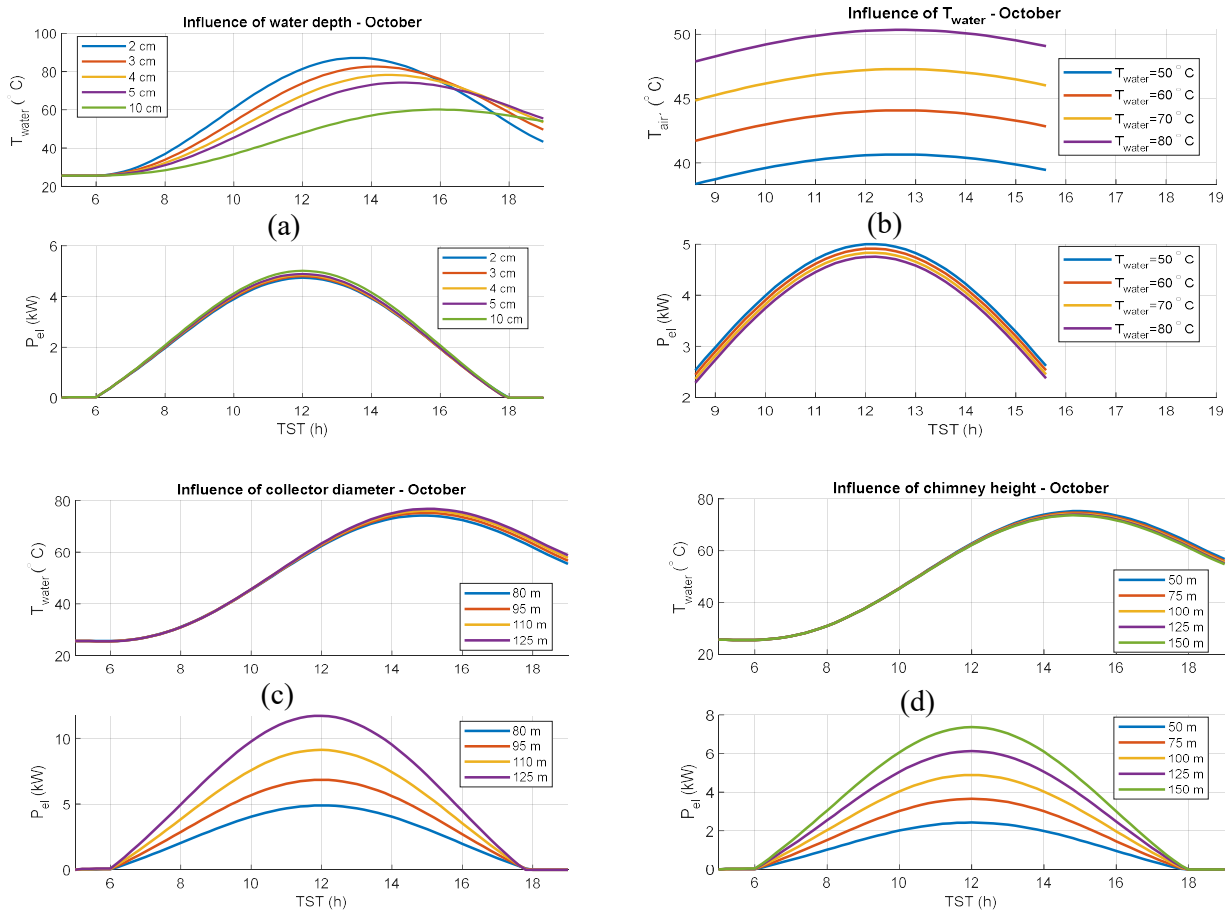


Figure 9: Influence of (a) water-layer thickness, (b) imposed main-air temperature, (c) collector diameter and (d) chimney height on simulated thermal and electrical performance in October

3.3. Estimation of process thermal-energy requirements from six trials

3.3.1. Comparative analysis of preheating temperature and electrical power

To identify favorable conditions for transferring preheated water to the external boiler, the water-temperature evolution of a 2 cm layer is compared with the electrical power produced by the plant for typical January and October days over 2010–2024.

In January, water temperature reaches 65 °C at around 12:16, while the calculated electrical power is 3.261 kW, or 99.86% of its daily maximum of 3.266 kW, reached at around 12:24. The proposed start of water withdrawal therefore occurs approximately eight minutes before the electrical peak. In October, withdrawal is scheduled to start at 12:00, when water temperature reaches 81.45 °C. At this time, electrical power also reaches its estimated daily maximum of 4.738 kW. The two quantities thus present simultaneously favorable conditions at the beginning of the operating period considered.

However, maximum water temperatures occur at approximately 14:00 in January and 13:36 in October, reaching 69.93 and 87.14 °C, respectively. This time difference reflects the thermal inertia of the water layer, whose temperature continues to increase after the electrical power peak.

International Journal of Progressive Sciences and Technologies (IJPSAT)
ISSN: 2509-0119.
© 2026 Scholar AI LLC.
https://ijpsat.org/
Vol. 60 No. 1 November 2026, pp. 528-555

These results allow water-withdrawal start times to be proposed according to the climatic conditions examined, prioritizing simultaneous availability of preheated water and high electrical power.

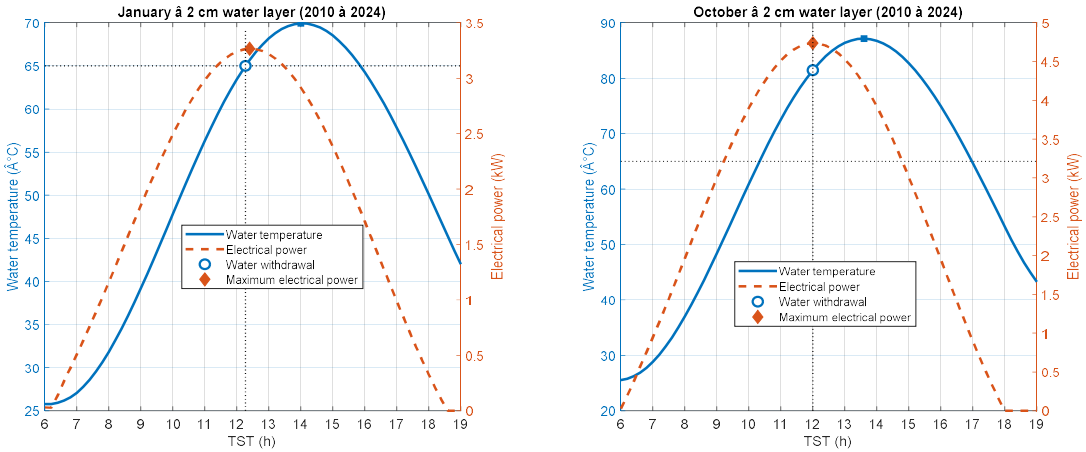


Figure 10: Simulated evolution of preheated-water temperature, water-withdrawal time and electrical power

3.3.2. Estimated heating energy and latent power for the six trials

The six experimental trials are used to determine the equivalent thermal requirements of the distillation process, distinguishing sensible heating from vaporization.

For an initial water mass of 250 kg, the sensible energy required to reach 100 °C is estimated at 10.16 kWh in January and 5.38 kWh in October. Adding 1.64 kWh for heating the metal shell and 0.234 kWh for thermal losses, the total thermal requirements reach 12.04 and 7.30 kWh, respectively, corresponding to a theoretical reduction of 40.46% in October.

Table 3 shows that equivalent average heating powers range from 8.70 to 19.00 kW in January and from 5.39 to 11.52 kW in October. The 156.5 kg Eucalyptus trial remains the most demanding in both scenarios, with an experimental heating duration of 38 min, and will be used as the reference for subsequent energy checks. Its latent vaporization power reaches 5.53 kW for an estimated steam flow rate of 8.82 kg·h⁻¹. Conversely, the 62 kg Eucalyptus trial has the lowest heating powers, 8.70 and 5.39 kW respectively, owing to its experimental heating duration of 85 min. Its latent vaporization power is also the lowest, at 0.68 kW.

Table 3: Estimated heating and vaporization thermal powers for the six trials.

Trials	Heating (min)	Extraction (min)	Condensate (L)	Flow rate (kg/h)	Pvap (kW)	Pheating Jan (kW)	Pheating Oct (kW)
Melaleuca 68 kg	49	141	16,5	7,02	4,40	14,82	9,03
Melaleuca 96 kg	50	140	7,7	3,30	2,07	14,53	8,86
Eucalyptus 156,5 kg	38	136	20,0	8,82	5,53	19,00	11,52
Eucalyptus 62 kg	85	195	3,5	1,08	0,68	8,70	5,39
Eucalyptus 80 kg	60	140	20,0	8,57	5,37	12,17	7,45
Cinnamomum 16 kg	62	114	7,0	3,68	2,31	11,79	7,23

International Journal of Progressive Sciences and Technologies (IJPSAT)
ISSN: 2509-0119.
© 2026 Scholar AI LLC.
https://ijpsat.org/
Vol. 60 No. 1 November 2026, pp. 528-555

Figure 11 thus highlights the effect of seasonal preheating conditions on heating requirements, whereas estimated vaporization powers remain the same for each trial. However, the initial solar configuration cannot meet the equivalent mean power required by the critical trial within the experimental durations considered. These results justify continuing geometric sizing of the plant based on time-dependent electricity-generation profiles.

The reduction in energy demand in October is mainly due to the higher initial temperature of preheated water, which reduces the sensible energy required to reach vaporization temperature. These results show that solar preheating significantly reduces the boiler's electrical demand during the heating phase.

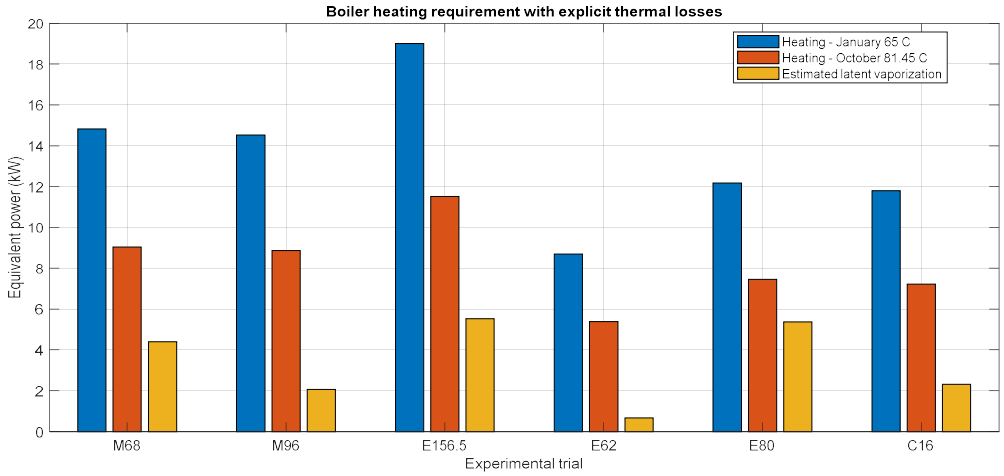


Figure 11: Equivalent boiler thermal requirements for the simulated preheating conditions in January and October and estimated latent powers during extraction.

3.3.3. Energy analysis of the distillation vessel

The distillation vessel has a useful volume above the perforated plate of approximately 1.480 m³. Apparent biomass loads range from 10.8 kg·m^{-3} for Cinnamomum (16 k) to 105.7 kg·m^{-3} for Eucalyptus (156.5 kg), corresponding to the highest volumetric loading observed (Table 4). Steam flow rates estimated from the condensates collected range from 1.08 to 8.82 kg·h^{-1}. The corresponding latent energies range from 2.19 to 12.54 kWh. The maximum values occur in the 156.5 and 80 kg Eucalyptus trials, whereas the minimum occurs in the 62 kg Eucalyptus trial. Per unit plant mass, specific energies range from 0.035 to 0.274 kWh·kg^{-1}. Cinnamomum has the highest specific energy and a better yield of 1%, while its volumetric load is the lowest. This high value is directly explained by the ratio between energy consumed and low plant mass and may also be affected by water-heating time, extraction time and steam flow rate.

An additional estimate of the sensible energy absorbed by the biomass assumes a specific heat capacity of 3.50 kJ·kg^{-1}·K^{-1} and an average heating from 30 to 90 °C. The results give energies between 0.93 and 9.13 kWh, the highest corresponding to the 156.5 kg Eucalyptus trial.

International Journal of Progressive Sciences and Technologies (IJPSAT)
ISSN: 2509-0119.
© 2026 Scholar AI LLC.
https://ijpsat.org/
Vol. 60 No. 1 November 2026, pp. 528-555

Table 4: Apparent loads and estimated energy indicators in the distillation vessel for the six trials

Trials	m_{vap} ($kg.h^{-1}$)	Apparent load ($kg.m^{-3}$)	E_ext (kWh)	E_sensible Biomass (kWh)	Especific ($kWh.kg^{-1}$)	R_{HE} (%)
Melaleuca 68 kg	7,02	45,9	10,34	3,93	0,152	0,22
Melaleuca 96 kg	3,30	64,9	4,83	5,60	0,050	0,17
Eucalyptus 156,5 kg	8,82	105,7	12,54	9,13	0,080	0,42
Eucalyptus 62 kg	1,08	41,9	2,19	3,62	0,035	0,65
Eucalyptus 80 kg	8,57	54,1	12,54	4,67	0,157	0,13
Cinnamomum 16 kg	3,68	10,8	4,39	0,93	0,274	1,00

.

These results show that the highest steam flow rate and/or volumetric loading do not necessarily correspond to the best extraction yield. Therefore, increasing thermal power or steam production alone cannot guarantee an improvement in essential oil yield. Process improvements must consider biomass load, steam flow rate and useful extraction duration jointly.

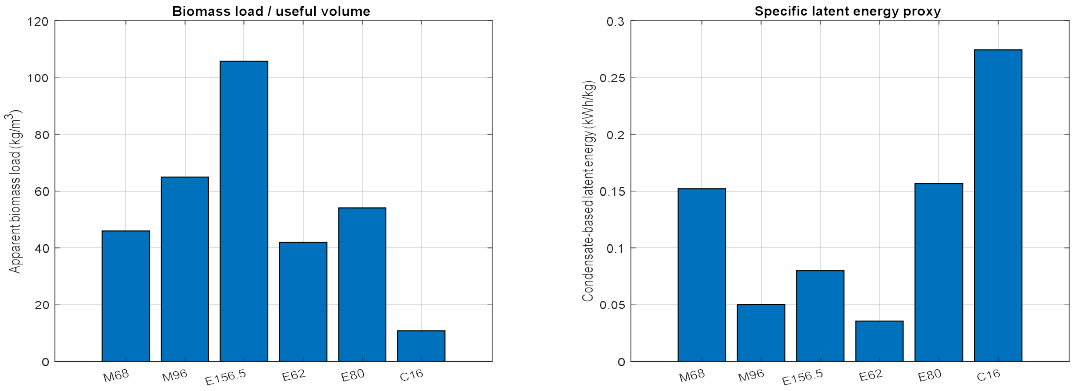


Figure 12: Biomass mass loading relative to the useful volume of the distillation vessel and estimated specific latent energy during extraction for the six trials

3.3.4. Energy analysis of the condenser

The experimental five-tube condenser has a total heat transfer area of approximately 0.1257 m². The open cooling-water tank has a geometric volume of approximately 232.5 L. Latent condensation powers range from 0.68 to 5.53 kW. Allowing for additional cooling of the condensate from 100 to 40 °C, the total thermal powers to be removed range from 0.75 to 6.15 kW. The most demanding case is the 156.5 kg Eucalyptus trial. For this trial, latent power reaches 5.53 kW and additional sensible power 0.61 kW, giving a total thermal load of 6.15 kW. Assuming a logarithmic mean temperature difference of 66.4 K, the overall heat transfer coefficient required for the five tubes is estimated at 737 $W \cdot m^{-2} \cdot K^{-1}$.

International Journal of Progressive Sciences and Technologies (IJPSAT)
ISSN: 2509-0119.
© 2026 Scholar AI LLC.
https://ijpsat.org/
Vol. 60 No. 1 November 2026, pp. 528-555

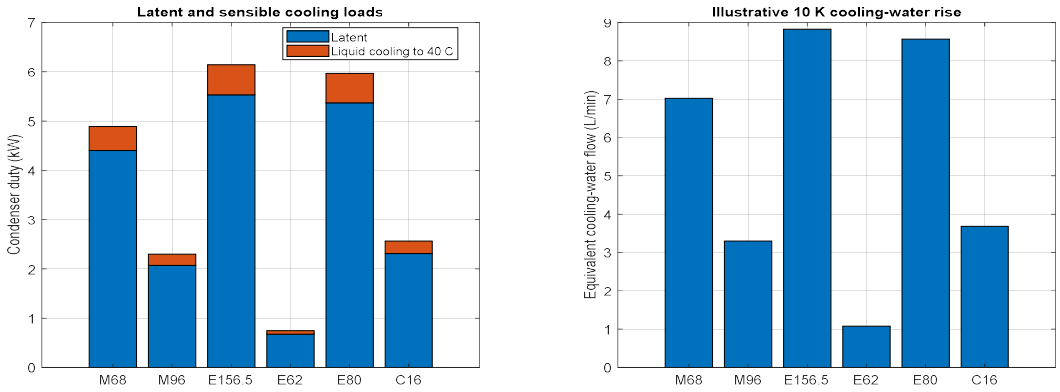


Figure 13: Estimated latent power to be removed for the six trials.

For an assumed condensate outlet temperature of 40 °C, Table 5 presents the thermal requirements and condenser sizing characteristics for the six experimental trials.

Table 5: Thermal requirements and preliminary condenser sizing for the six experimental trials

Trial	P_ lat (kW)	P_sens (kW)	P_tot (kW)	V_water (L)	U_tot (W·m⁻²·K⁻¹)	N_tubes
Melaleuca 68 kg	4,40	0,49	4,89	989,92	586,18	8
Melaleuca 96 kg	2,07	0,23	2,30	461,96	275,5	4
Eucalyptus 156,5 kg	5,53	0,61	6,15	1199,9	736,64	10
Eucalyptus 62 kg	0,68	0,08	0,75	209,98	89,90	2
Eucalyptus 80 kg	5,37	0,60	5,97	1199,9	715,59	10
Cinnamomum 16 kg	2,31	0,26	2,57	419,97	307,58	5

A sensitivity analysis of condenser outlet temperature was conducted between 30 and 70 °C for the critical case.

Table 6: Effect of final condensate temperature on thermal load and cooling-water flow rate

Tcond (°C)	Qsensible (kW)	Qtotal (kW)	Water flow ΔT=10 K (L/min)	Water /136 min (L)	Basin renewals
30	0.72	6.25	8.97	1220	5.25
40	0.61	6.15	8.82	1200	5.16
50	0.51	6.04	8.68	1180	5.07
60	0.41	5.94	8.53	1160	4.99
70	0.31	5.84	8.38	1140	4.90

For an outlet temperature scenario of 40 °C and a 10 K temperature rise in cooling water, water demand is approximately 8.8 L·min⁻¹. Over 136 min, this represents about 1.2 m³ of water, or approximately 5.16 times the tank's geometric volume of 232.5 L. Water replacement or circulation becomes a decisive parameter.

International Journal of Progressive Sciences and Technologies (IJPSAT)
ISSN: 2509-0119.
© 2026 Scholar AI LLC.
https://ijpsat.org/
Vol. 60 No. 1 November 2026, pp. 528-555

Table 7: Cooling-water flow rates and cumulative volumes according to temperature rise

ΔT water (K)	Water flow (L/min)	Volume over 136 min (L)	Basin renewals
5	17.65	2400	10.32
10	8.82	1200	5.16
15	5.88	800	3.44
20	4.41	600	2.58

3.4. Sizing of the solar chimney power plant according to the six experimental trials

Analysis of the three subcomponents clearly distinguishes two successive constraints: an energy constraint during heating and a power constraint during extraction. The calculations retain an initial water load of 250 kg, the specific experimental durations of each trial and an assumed complete conversion of electrical energy to resistive heat.

Water-withdrawal times are set at 12:16 TST in January and 12:00 TST in October. Reference preheating temperatures are 65 °C and 81.45 °C, respectively, for a 2 cm water layer.

3.4.1. Minimum dimensions for the six trials

Table 8 summarizes the minimum dimensions determined for each trial under the two climatic scenarios, with a 15% margin and the sensitivity scenario for extraction power.

Table 8: Minimum collector and chimney dimensions for the six experimental trials

Trial	D_col Jan (m)	H_chem Jan (m)	D_col Oct (m)	H_chem Oct (m)
Melaleuca 68 kg	165	131,6	130	103,7
Melaleuca 96 kg	165	131,6	125	99,7
Eucalyptus 156,5 kg	180	143,6	135	107,7
Eucalyptus 62 kg	140	111,7	130	103,7
Eucalyptus 80 kg	155	123,6	140	111,7
Cinnamomum 16 kg	155	123,6	115	91,7

In January, minimum diameters range from 140 to 180 m; in October, they range from 115 to 140 m. The most demanding geometry is imposed by the 156.5 kg Eucalyptus trial in January, with a collector diameter of 180 m and chimney height of 143.6 m. The difference between the two months is explained by the more favorable solar potential and higher preheating temperature adopted for October.

3.4.2. Verification of the common configuration

The minimum common configuration satisfying all six trials in both months, under the selected geometric ratio and 15% margin, is D_col = 180 m and H_chem = 143.6 m. It corresponds to a collector area of approximately 25,447 m². For the sizing 156.5 kg Eucalyptus trial, the electrical energy generated during 38 min of heating reaches 14.07 kWh in January for an estimated requirement of 12.03 kWh, yielding a gross margin of 16.9%. In October, the energy available over the same duration reaches 20.35 kWh for a requirement of 7.30 kWh, a gross margin of 178.9%. Maximum daily electrical powers are 22.34 and 32.45 kW, respectively. During extraction, simulated minimum electrical powers are 14.85 kW in January and 20.29 kW in October. They

International Journal of Progressive Sciences and Technologies (IJPSAT)
ISSN: 2509-0119.
© 2026 Scholar AI LLC.
https://ijpsat.org/
Vol. 60 No. 1 November 2026, pp. 528-555

remain above the verification threshold of approximately 8.34 kW, corresponding to an assumed extraction power of 7.25 kW increased by a 15% margin.

Table 9: Energy verification of the common configuration for 156.5 kg Eucalyptus

Indicator	January	October
Required heating energy (kWh)	12,03	7,30
Energy available during 38 min (kWh)	14,07	20,35
Gross heating margin (%)	16,9	178,9
Maximum electrical power (kW)	22,34	32,45
Minimum power during extraction (kW)	14,85	20,29
Assumed extraction power (kW)	7,25	7,25

These results show that the selected configuration numerically meets the two successive energy constraints under the simulated conditions. Thus, the 180/143.6 m configuration is a numerically admissible solution for all six trials.

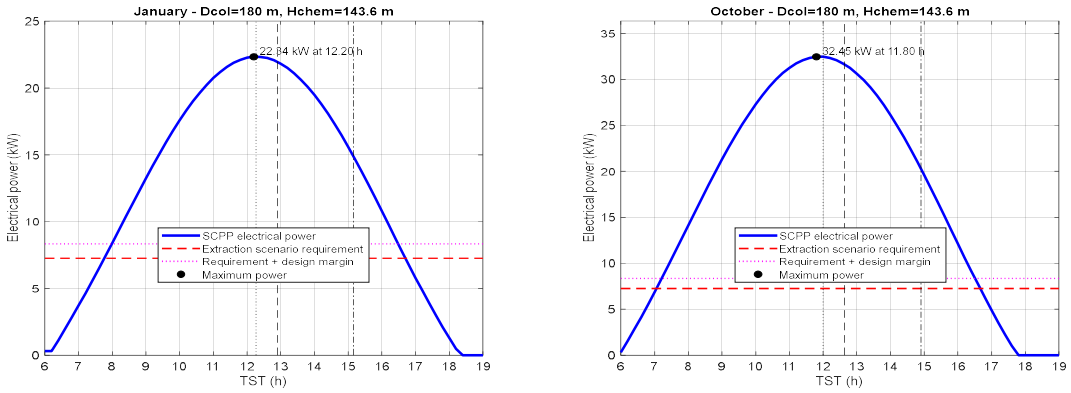


Figure 14: Time evolution of the simulated electrical power of the common 180 m / 143.6 m configuration.

3.5. Process improvement and final resizing

The improvement aims to reduce the dimensions of the solar chimney power plant while satisfying the successive heating and extraction stages of the six trials. Drawn from the literature [40], [41], the selected strategy combines reducing the initial boiler water from 250 to 125 L, setting heating at 90 min, setting extraction durations to 180 min for the three plants, and using a 1 cm water layer in the collector. The electric-to-thermal conversion efficiency of the resistance heater is taken as 100%, with boiler losses estimated separately.

3.5.1. Choice of water layer and temporal optimization

The comparative study of thicknesses of 1, 1.5 and 2 cm shows that the 1 cm layer reaches the 65 °C threshold at about 11:13 in January, versus 11:44 for 1.5 cm and 12:16 for 2 cm. However, the improvement criterion is not to maximize water temperature. Earlier withdrawal increases the electrical heating demand but allows extraction to finish before the late decline in solar power. A common withdrawal time of 9:24 TST was therefore examined for the configuration with a diameter of 165 m and height of 131.6 m. At this time, simulated temperatures in January are 50.62 °C, 46.24 °C and 43.04 °C for 1, 1.5 and 2 cm, respectively. In October, they reach 65.92 °C, 59.49 °C and 54.56 °C. This result supports the numerical choice of 1 cm for early withdrawal.

International Journal of Progressive Sciences and Technologies (IJPSAT)
ISSN: 2509-0119.
© 2026 Scholar AI LLC.
https://ijpsat.org/
Vol. 60 No. 1 November 2026, pp. 528-555

3.5.2. Results of earlier water withdrawal

Table 10: Operating balance of the critical 156.5 kg Eucalyptus trial with the improved candidate configuration (Dcol = 165 m; Hchem = 131.6 m; heau = 1 cm; t0 = 9:24 TST).

Indicator	January	October
Basin temperature at 9:24	50,62 °C	65,92 °C
Electrical energy required for heating	9,29 kWh	7,15 kWh
Electrical energy available during 90 min	19,90 kWh	30,98 kWh
Minimum power during 180 min of extraction	15,05 kW	20,46 kW
Extraction threshold with 15% margin	8,34 kW	8,34 kW
End of heating	10 h 54 TSV	10 h 54 TSV
End of critical extraction	13 h 54 TSV	13 h 54 TSV

In January, earlier withdrawal lowers the temperature from 65.71 °C (at 10:48) to 50.62 °C (at 9:24), increasing heating energy from 7.18 to 9.29 kWh. Nevertheless, the 19.90 kWh available over 90 min covers this requirement with the selected margin. More importantly, the minimum power during the 180 min extraction period increases from 11.07 to 15.05 kW, because extraction ends at 13:54. In October, at 9:24, simulated water temperature reaches 65.92 °C. Required heating energy is 7.15 kWh, compared with 30.98 kWh available. Minimum power during extraction is 20.46 kW.

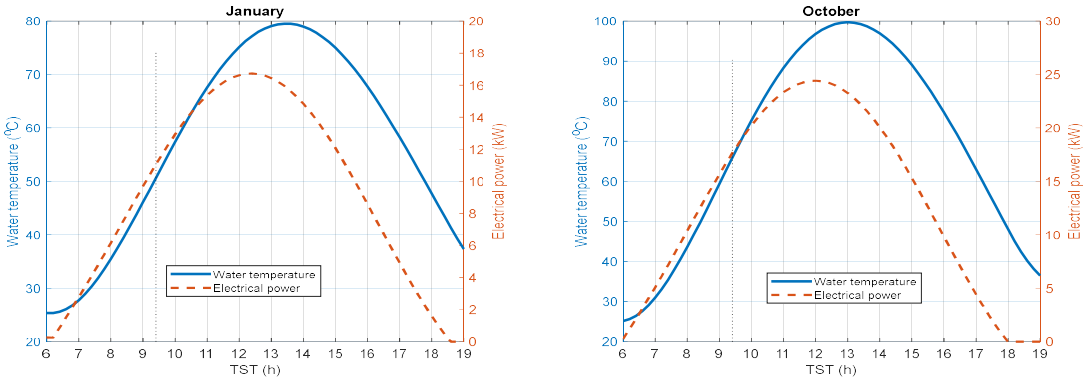


Figure 15: Simulated basin temperature and electrical power in January and October; water withdrawal at 9:24

3.5.3. Summary comparison of the reference and improved configurations

Table 11: Comparison of geometric and energy parameters of the reference and final improved configurations.

Parameter	Reference	Improved	Change
Collector diameter (m)	180	165	−8,3 %
Chimney height (m)	143,6	131,6	−8,4 %
Collector area (m²)	25 447	21 382	−16,0 %
Water-layer thickness (cm)	2	1	−50 %
Boiler water volume (L)	250	125	−50 %
Heating duration of the critical trial (min)	38	90	+52 min
Start of withdrawal in January (TST)	12 h 16	9 h 24	−2 h 52
Temperature at withdrawal in January (°C)	65,00	50,62	−14,38 °C
Start of withdrawal in October (TST)	12 h 00	9 h 24	−2 h 36
Temperature at withdrawal in October (°C)	81,45	65,92	−15,53 °C
Heating energy, critical case, January (kWh)	12,03	9,29	−22,8 %
Critical-case extraction (min)	136	180	+44 min
End of extraction in January (TST)	15 h 10	13 h 54	−1 h 16
Minimum extraction power, January (kW)	14,85	15,05	+1,3 %
Resistance heater electric-to-thermal conversion (%)	100	100	Unchanged

Table 10 highlights a reduction in diameter from 180 to 165 m and in height from 143.6 to 131.6 m, corresponding to an approximately 16.0% reduction in collector area. This improvement results from reducing the water layer from 2 to 1 cm, reducing the initial boiler load from 250 to 125 L, and advancing the withdrawal time.

In January, transfer temperature decreases from 65.00 to 50.62 °C, but heating energy for the critical case falls from 12.03 to 9.29 kWh owing to the reduced water mass and new heating window. Despite increasing the critical extraction time from 136 to 180 min, the end of the cycle is brought forward from 15:10 to 13:54 TST. Minimum electrical power available during extraction reaches 15.05 kW, compared with 14.85 kW for the reference. The new configuration meets the model criteria in the scenarios studied.

4. CONCLUSION

This study assessed the energy performance and optimization of a solar chimney power plant intended to supply electricity to an essential oil extraction still under the climatic conditions of Mahajanga. It combines thermal and electrical modeling of the plant with six experimental distillation trials to compare solar generation against the successive energy requirements of the process. Energy analysis of the experimental trials identified the 156.5 kg Eucalyptus trial as the sizing case, with an estimated mean steam flow rate of 8.82 kg·h^{-1} and corresponding latent power of 5.53 kW. For a 2 cm water layer and an initial boiler load of 250 L, reference sizing results in a collector 180 m in diameter and a chimney 143.6 m high. This configuration reaches simulated peak electrical powers of 22.34 kW in January and 32.45 kW in October, confirming the influence of climatic conditions on plant electricity generation. Process improvement involves reducing the boiler water volume from 250 to 125 L,

adopting a 90 min heating period and adapting extraction durations. The comparative study of thicknesses of 1, 1.5 and 2 cm showed that a 1 cm water layer makes it possible to reach useful preheating temperatures earlier. Advancing water withdrawal to 9:24 TST is also an important temporal optimization lever, avoiding unnecessary waiting for the maximum water temperature. The improved configuration has a 165 m diameter collector and a 131.6 m high chimney, corresponding to a 16.0 % reduction in collector area relative to reference sizing. For the critical 156.5 kg Eucalyptus trial, the water temperature at withdrawal reaches 50.62 °C in January and 65.92 °C in October. Despite these differing temperatures, the electrical energies available during heating, 19.90 and 30.98 kWh respectively, exceed estimated requirements of 9.29 and 7.15 kWh. During the 180 min extraction period, minimum available electrical powers reach 15.05 kW in January and 20.46 kW in October, exceeding the adopted sizing threshold of 8.34 kW for the critical case, including margin. The comparison thus reveals more favorable operating conditions in October, while the configuration remains admissible in January under the numerical assumptions. The principal scientific contribution of this study lies in the numerical demonstration that better management of preheating, water quantity and operating times can reduce plant dimensions while maintaining a favorable energy match with the still's requirements. Optimization therefore involves not only increasing electricity generation but also jointly adapting plant characteristics and process operating conditions. Nevertheless, the feasibility obtained remains conditional on the model assumptions. Research prospects mainly concern experimental validation of the model, measurement of power actually consumed by the still, investigation of preheated-water transfer, and techno-economic and structural analysis of the improved plant before any large-scale implementation.

REFERENCES

[1] Grand View Research, estimations de marché des huiles essentielles (croissance du marché mondial).

[2] Barbieri, C., & Borsotto, P. (2018). Essential oils: market and opportunities. In « Potential of Essential Oils ». IntechOpen.

[3] Market analyses (CAGR ~9 % 2021–2028).

[4] Trilles, B., et al. Études sur le Niaouli de Madagascar (composition et production).

[5] Travaux sur le Ravintsara (*Cinnamomum camphora*) à Madagascar (rendements et distillation).

[6] Pise, V. H., & Thorat, B. N. (2023). Green steam for sustainable extraction of essential oils using solar steam generator. Sustainable Chemistry and Pharmacy.

[7] Études LCA sur la distillation à la vapeur (consommation énergétique et émissions).

[8] Comparaisons distillation bois vs solaire (émissions de CO_2 et efficacité).

[9] Schlaich, J., Bergermann, R., Schiel, W., & Weinrebe, G. (2005). Design of commercial solar updraft tower systems. Journal of Solar Energy Engineering, 127(1), 117–124.

[10] von Backström, T. W., & Gannon, A. J. (2000). Compressible flow through solar chimney power plant collectors. Journal of Solar Energy Engineering, 122(3), 133–137.

[11] von Backström, T. W., & Gannon, A. J. (2003). Solar chimney turbine characteristics. Solar Energy, 76, 235–241.

[12] Kreetz, H. (1997). Theoretische Untersuchungen und Auslegung eines Aufwindkraftwerks mit Wasserspeicher. TU Berlin.

[13] dos Santos Bernardes, M. A., et al. (2013). Analysis of some available heat transfer coefficients applicable to solar chimney power plant collectors. Solar Energy.

[14] Semai, H. Recherche d'une configuration optimale d'une centrale solaire à cheminée. Thèse de doctorat, Faculté des Sciences, Département de Physique.

[15] Bergman, T. L., Lavine, A. S., Incropera, F. P., & DeWitt, D. P. Fundamentals of Heat and Mass Transfer.

[16] MacAdams, W. H. (1954). Heat Transmission.

[17] Khalilian, M. (2017). Experimental investigation and theoretical modelling of heat transfer in circular solar ponds by lumped capacitance model. Applied Thermal Engineering, 121, 737–749.

[18] Gortych, M., Lipnicki, Z., Małolepszy, T., & Grabas, P. (2024). Solar Chimney Operation Variant. Energies, 17(19), 5004.

[19] Hollands, K. G. T., Raithby, G. D., & Konicek, L. (1975). International Journal of Heat and Mass Transfer, 18(7–8), 879–884.

[20] Koonsrisuk, A., & Chitsomboon, T. (2013). Mathematical modeling of solar chimney power plants. Energy, 51, 314–32

[21] Bernardes, M. A. dos S., Voß, A., & Weinrebe, G. (2003). Thermal and technical analyses of solar chimneys. Solar Energy, 75(6), 511–524

[22] Schlaich, J., Bergermann, R., Schiel, W., & Weinrebe, G. (2005). Design of commercial solar updraft tower systems—Utilization of solar induced convective flows for power generation. Journal of Solar Energy Engineering, 127(1), 117–124

[23] Dai YJ, Huang HB, Wang NRZ. Case study of solar chimney power plants in North-western regions of China. Renewable Energy 2003; 28: 1295-304.

[24] Soukaina HILALI, Thermal solar energy applications on ecoextraction and drying of orange peels and rosemary leaves, 2020

[25] R. BARISON James, Production d'electricite par une cheminee solaire, Memoire, Université d'Antananarivo, 2012.

[26] ACHOURI El Hadj, Contribution à l'étude expérimentale d'une cheminée solaire en Algérie, these de doctorat, Université Kasdi Merbah Ouargla, 2021

[27] Bergman, T. L., Lavine, A. S., Incropera, F. P., & DeWitt, D. P. Fundamentals of Heat and Mass Transfer. (Formule de surface d'échange d'un faisceau tubulaire).

[28] Farooq et al. (2015) — Grey-box modeling of a low pressure electric boiler for domestic hot water system. Applied Thermal Engineering, 84, 257–267.

[29] Bergman, Lavine, Incropera et DeWitt (2018) — Fundamentals of Heat and Mass Transfer, 8e édition, Wiley, chapitre 5 : Transient Conduction, sections 5.1–5.3.

[30] Harvey, A. H. (1998). Thermodynamic properties of water: Tabulation from the IAPWS formulation 1995 for the thermodynamic properties of ordinary water substance for general and scientific use. NISTIR 5078.

[31] Bird, Stewart et Lightfoot, Transport Phenomena, 2e édition, chapitre 6, Bird et al. (2002), Transport Phenomena

[32] Choi, Y. et Okos, M. R. (1986), Effects of temperature and composition on the thermal properties of foods, Food Engineering and Process Applications, vol. 1, p. 93–101.

[33] Australian Stainless Steel Development Association, 304: The Place to Start, propriétés thermophysiques de l'acier inoxydable 304

[34] Cassel et al. (2009), Steam distillation modeling for essential oil extraction process, Industrial Crops and Products, 29(1), 171–176.

[35] Nusselt, W. (1916), théorie de la condensation en film sur tube horizontal (couverte dans Bergman/Incropera et confirmée comme référence la plus fiable par les comparatifs récents de corrélations)

[36] ASHRAE. ASHRAE Handbook — Fundamentals, chapitre « Heat Transfer », section « Heat Exchangers — Mean Temperature Difference Analysis

[37] Franco, A. (2020). Methods for the sustainable design of solar energy systems for industrial process heat. Sustainability, 12(12), 5127.

[38] Schoeneberger, C. A., et al. (2020). Solar for industrial process heat: A review of technologies, analysis approaches, and potential applications in the United States. Energy, 206, 118083.

[39] National Renewable Energy Laboratory. System Advisor Model — Electric Load.

[40] Pipatpaiboon and al. (2025). Improving the Efficiency of Essential Oil Distillation via Recurrent Water and Steam Distillation: Application of a 500-L Prototype Distillation Machine and Different Raw Material Packing Grids. AgriEngineering, 7, 175.

[41] Setiawan S., Nadhilah A., Ilhamsari R.P. (2022). Effects of Leaf Storage and Distillation Time on the Quality of Eucalyptus (Eucalyptus grandis) Essential Oil. 3BIO: Journal of Biological Science, Technology and Management, 4(1).